JOURNAL OF Materials CHEMISTRY

Structural study of 3D-hexagonal mesoporous spin-coated sol–gel films

Sophie Besson,[a,b] Thierry Gacoin,[a] Catherine Jacquiod,[b] Christian Ricolleau,[c] David Babonneau[d] and Jean-Pierre Boilot*[a]

[a]*Groupe de Chimie du Solide, Laboratoire de Physique de la Matière Condensée, UMR CNRS 7643, Ecole Polytechnique, 91128 Palaiseau, France*
[b]*Laboratoire CNRS/Saint-Gobain "Surface du Verre et Interfaces", UMR CNRS 125, 39 quai Lucien Lefranc, 93303 Aubervilliers, France*
[c]*Laboratoire de Minéralogie Cristallographie, UMR CNRS 7590, Universités Paris VI et Paris VII, 4 place Jussieu, 75252 Paris cedex 05, France*
[d]*Laboratoire de Métallurgie Physique, UMR CNRS 6630, Université de Poitiers, UFR Sciences SP2MI, Téléport 2, Bd Marie et Pierre Curie BP 30179, 86962 Futuroscope Chasseneuil Cedex, France*

Received 8th November 1999, Accepted 21st March 2000
Published on the Web 10th May 2000

Mesostructured films deposited on glass substrates by spin coating are studied by X-ray diffraction, small angle X-ray scattering using grazing incidence (GISAXS) and high resolution electron microscopy. The films generally present a gradient of ordering from the air/sol interface to the interior of the film, with a 3D-hexagonal mesophase near the surface and a disordered micellar structure at the interior. However, the 3D-hexagonal ordering and the texturing can be extended over all the film thickness by adjusting the composition of the deposited solution. In particular, critical values are clearly observed both for the size of silica units forming the walls in the mesophase and for the film thickness. All these results can be understood from the competition between structuration and gelation of the films during alcohol removal.

1 Introduction

Materials with periodic mesoscale spaces, synthesized through the reactions of inorganic species in the presence of surfactant assemblies, have attracted worldwide attention since the discovery of MCM-41.[1,2] A wide variety of mesophases with different compositions and structures have been obtained by the modification of the synthesis conditions, including inorganic species, surfactants and reaction conditions.[3–5] The materials have generally amorphous, silica-based frameworks with highly regular arrays of uniform-sized channels whose diameters can be tailored in the range from 2 to over 10 nm through the choice of linear cationic surfactant molecules used in their preparation. The pores in these materials are nearly as regular, yet considerably larger, than have been achieved in zeolites, and afford new opportunities in catalysis and chemical separation.[4] These materials are also expected to be applied to electrical and optical devices through the incorporation of various guest species.

However, since most of these materials are powders, the control of the morphology, especially film forming, is a key issue for practical applications. Above a critical micelle concentration, mesoporous silica films can be slowly grown at solid–liquid and liquid–vapor interfaces through an interfacial silica–surfactant self-assembly process.[6,7] More recently, the rapid formation of supported mesoporous transparent films by spin- and dip-coating sol–gel techniques has been reported.[8–11] Especially, Lu *et al.*[10] and Zhao *et al.*[11] have shown the formation of cubic mesoporous films, in which the pores are interconnected in a three-dimensional network that allows their accessibility from the film surface.

Finally, we have recently observed the formation of a 3D-hexagonal structure in sol–gel mesoporous silica films spin coated on conventional glass plates.[12] This structure results from the three-dimensional hexagonal arrangement of spherical micelles separated by silica walls. In this paper, the structural study of the 3D-hexagonal spin-coated sol–gel films is essentially performed by X-ray diffraction and small angle X-ray scattering using grazing incidence. We show how the extent of ordering and texturing can be optimized in these films by varying the composition of the deposited solution. All the results are understood from a simple mechanism related to the competition between structuration and gelation of the films during alcohol removal.

2 Experimental

Precursor solutions were prepared by addition of a cationic surfactant (CTAB: $CH_3(CH_2)_{15}N^+(CH_3)_3Br^-$) to polymeric sols made in acidic conditions. In a typical sol preparation, TEOS ($Si(OC_2H_5)_4$), water (pH = 1.25 with HCl) and ethanol (mole ratio 1 : 5 : 3.8) were mixed. After magnetic stirring at 25 °C, the sols were aged at 40 or 60 °C for different times (from 30 minutes to 23 hours). Under these conditions, and whatever the aging time, ^{13}C NMR spectra clearly show the complete hydrolysis of the ethoxy groups. CTAB was then ultrasonically mixed into the sol, which can be eventually diluted with ethanol (from 1 : 1 to 1 : 27). The CTAB/Si molar ratio (equal to 0.1) was chosen in order to obtain the previously described 3D-hexagonal mesophase.[12] Afterwards, the as-prepared mixture was passed through a 0.45 μm filter and spin-coated in air on glass plates. Prior to deposition, the glass plates were ultrasonically cleaned in detergent, distilled water and deionized water for 15 min, respectively, followed by drying in a flow of nitrogen. The angular velocity range of the spinner was 2000 rpm. After deposition the sample plates were dried in air at room temperature for one day. Calcined films were obtained by heating in air at 400 °C for 12 hours, which ensures complete removal of organic species. The film thickness (before

and after calcination) was estimated using a Sloan Dektak III ST stylus profilometer.

The structure and texture of the films were characterized by X-ray diffraction (XRD), in the Bragg–Brentano geometry, using CuKα radiation (8.049 keV). Whatever the experimental conditions used, the spectra are consistent with the previously observed hexagonal structure. The indexations are given in the 3D hexagonal system ($P6_3/mmc$ space group). The presence of only 002 and 004 low angle reflections (the *hkl* reflections with *h* or $k \neq 0$ are missing) suggests that the film has a highly textured 3D hexagonal mesostructure with the *c*-hexagonal axis perpendicular to the film plane. The coherence lengths were determined from the width of the 002 peak using Scherrer's law.

Further structural data were obtained from grazing incidence small angle X-ray scattering (GISAXS) measurements.[13,14] These were made at the French synchrotron radiation source LURE-DCI (D22 station). Two sets of experiments were performed concerning the aging of the silica sol (set 1) and the dilution of the CTAB/sol mixture (set 2). The chosen energies were 8 and 7 keV for sets 1 and 2, respectively. The samples were positioned with their surface quasi-parallel to the X-ray beam. The angle of incidence, α, was considered close to the critical angle for total reflection α_c, when the intensity of the reflected beam was reduced by 50% with respect to that of the incoming beam. The scattering patterns were recorded with a 2D detector set perpendicular to the incident beam. The distances between the sample and the recording plane were 700 and 500 mm in sets 1 and 2, respectively. As shown in Fig. 1, less than the upper half part of the scattering can be observed because of the shadow of the sample. The specular and off-specular scattered intensities at very low angles due to surface roughness are not taken into account here because they are masked thanks to a vertical beam-stop. Hereafter, the scattering vector $\boldsymbol{q}$ is reduced into two components: $\boldsymbol{q}=\boldsymbol{q}_y+\boldsymbol{q}_z$, where $\boldsymbol{q}_y$ and $\boldsymbol{q}_z$ are the horizontal and vertical components, respectively. The modulus of $\boldsymbol{q}$ is $4\pi \sin\theta/\lambda$ where θ equals half the scattering angle and λ equals the wavelength of the incident radiation (0.155 and 0.177 nm for sets 1 and 2, respectively).

High-resolution electron microscopy (HRTEM) investigations were made using a Philips CM20 electron microscope operating at 200 kV with a point to point resolution $r=0.27$ nm. The 3D order within the silica mesoporous films was studied by examining the films in cross section. The cross section samples were prepared by cutting thin strips of film on substrate material and by cementing two films face to face. The thinning process was achieved by mechanical polishing and ion milling until the suitable thickness for electron transparency was reached. Using such specimen preparation, the electron beam is parallel to the interface plane between the glass substrate and the silica film in order to be able to observe the whole film thickness.

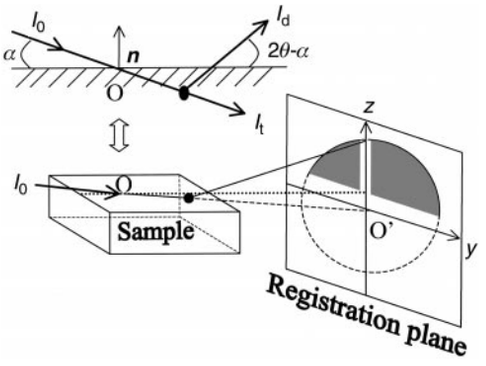

Fig. 1 Principle of grazing incidence small-angle X-ray scattering (GISAXS).

3 Results

We first studied films prepared from silica sols subjected to different aging times at 40 °C. The film thickness is nearly constant whatever the sol, and changes from 1000 to 800 nm upon calcination. This is due to the removal of the surfactant template from the spheres concomitant with the condensation of silanol groups in the walls. Fig. 2 shows the evolution of the 002 peak as a function of the aging time of the silica sol. In all cases, as expected from previous studies on mesoporous structures, a large contraction (about 23%) of the $d_{(002)}$ spacing is observed upon calcination in agreement with the decrease of the film thickness (20%). We note, both before and after calcination at 400 °C, a steady decrease in the $d_{(002)}$ spacing (from 4.1 to 3.7 nm and from 3.2 to 2.8 nm, respectively) when the aging time increases (from 30 minutes to 23 hours). Another point, already reported by Ryoo *et al.* for MCM41-type films,[15–17] is the clear evidence of an optimum of the sol condensation for the film structuration. Both for short (1 hour) and long (23 hours) aging times of the silica sol at 40 °C, the broad 002 lines correspond to a coherence length of about 20–30 nm. This contrasts with the sharp intense peaks observed in the optimum condensation range (between two and six hours) corresponding to large ordered domains (the experimental coherence length is then superior to the instrumental resolution, *i.e.* 110 nm). Note also that the optimum range, as the condensation kinetics, is obviously temperature dependent. Thus, silica sol aging for only 30 minutes at 60 °C leads to an optimized ordering.

Fig. 3 shows GISAXS patterns recorded on uncalcined films prepared with sols of different aging times. For $\alpha=\alpha_c$, the refracted beam propagates quasi-parallel to the surface of the film and it can be considered as a primary beam for small angle scattering. For a wavelength of 0.155 nm, a penetration depth z_o of 50 nm is deduced from the complex refractive index of the film, which is determined by reflectometry measurements. Consequently, under these conditions, the SAXS signal essentially gives information on the structure at the film/air interface. When the incident beam is slightly larger ($\alpha=\alpha_c+0.05°$), the refracted beam penetrates the layer

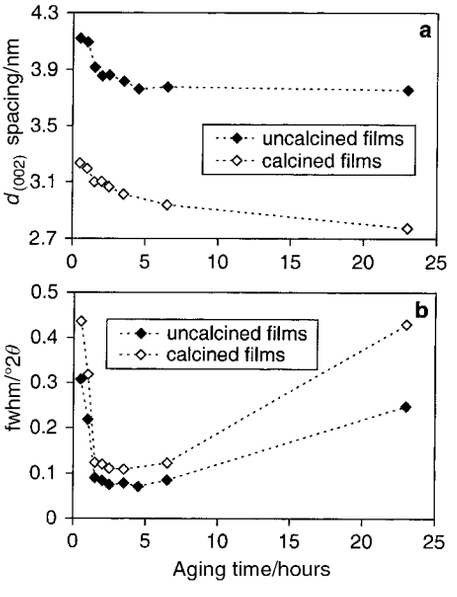

Fig. 2 X-Ray diffraction data deduced from patterns obtained from mesostructured films in the Bragg–Brentano geometry (CuKα): evolution of the 002 diffraction peak (a. $d_{(002)}$ spacing; b. width) as a function of the aging time at 40 °C for the silica sol. Between two and six hours the width of the peak corresponds to the instrumental resolution.

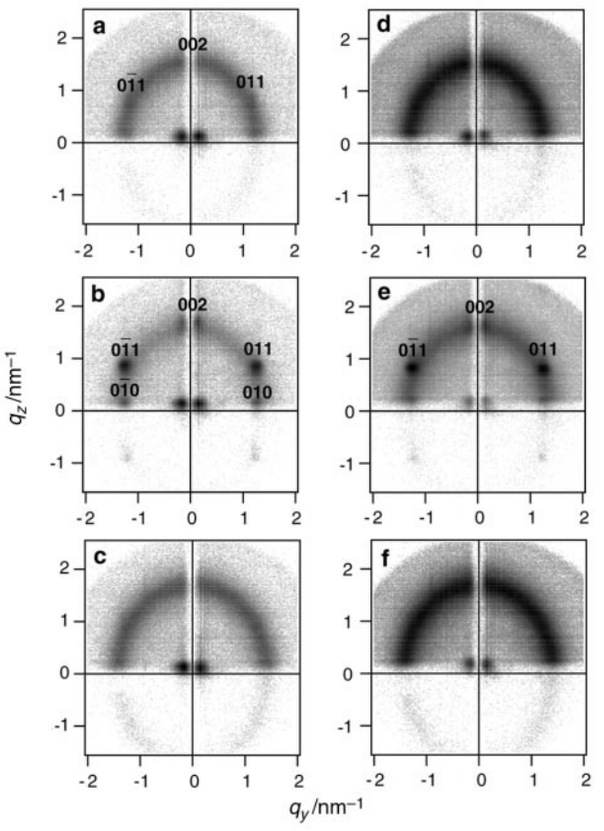

Fig. 3 GISAXS patterns recorded at different angles of incidence (α) for uncalcined mesostructured films prepared from silica sols with different aging times (t) at 40 °C : a ($\alpha=\alpha_c$, $t=1$ h); b ($\alpha=\alpha_c$, $t=4.5$ h); c ($\alpha=\alpha_c$, $t=23$ h); d ($\alpha=\alpha_c+0.05°$, $t=1$ h); e ($\alpha=\alpha_c+0.05°$, $t=4.5$ h); f ($\alpha=\alpha_c+0.05°$, $t=23$ h).

($z_o=400$ nm) and the SAXS signal gives information on the structure at the interior of the film.

Three types of repartition for the X-ray diffuse scattering can be clearly observed on the patterns. Their relative intensity depends both on the α value and on the aging time of the sol.

First, near the surface of the film and more pronounced in the optimum range of condensation, we observe Bragg diffraction spots which can be hexagonally indexed as the 002, 010, 011, $0\bar{1}0$ and $0\bar{1}1$ reflections corresponding to the $[2\bar{1}0]$ zone axis orientation for the 3D hexagonal structure. This direct view of the reciprocal space confirms the hexagonal array in the near surface region with the c axis perpendicular to the film surface.

Second, for a well-structured film (4.5 hours of aging at 40 °C for the sol) and more pronounced at the interior, diffuse lines are observed between Bragg spots showing a disorder due to small displacements of spheres from their nominal position in the hexagonal lattice. This indicates the existence of some disordered regions that retain an average hexagonal local order.

Third, at the interior of the film and more pronounced outside the optimum range, a diffuse halo is observed whose ellipsoid shape indicates a distribution of distances between spherical micelles throughout the film. In fact, the halo crosses over the 002, 010 and $0\bar{1}0$ Bragg diffraction spots showing that the neighbor separations between micelles are retained in the disordered part of the film, both in y and z directions.

Besides the clear evidence of an optimum for the condensation of silica sols, GISAXS results also confirm the growth of ordered domains from the air–sol interface towards the interior of the film. This is in agreement with the model proposed by Yang *et al.*[6] for MCM41-type films grown at the air–liquid interface, which assumes that the formation of a mesostructured silica film involves collective interactions between silica–surfactant micellar species and a surfactant overstructure that self-assembles the air–sol interface at an earlier stage of the deposition process.

Moreover, in agreement with transmission electron microscopy (TEM) observations (Fig. 6a, see later) and contrasting with dip-coated films deposited on silicon substrates,[10] we have no evidence of the presence of an ordered region near the glass plate. Consequently, the film structure can be described as an ordered region of 3D-hexagonal mesophase at the surface and a disordered micellar structure (disordered spherical micelles) at the interior of the film.

Finally, the last structural information, which allows one to interpret the shift of the 002 line on the $\theta-2\theta$ diffraction patterns as a function of the condensation time, is given by a complete analysis of the Bragg spot positions on the GISAXS patterns. The determination of the q_z and q_y coordinates for the 011 and $0\bar{1}1$ peaks leads to a c/a ratio of the lattice spacing which is largely inferior (about 30%) to the expected value for the hexagonal close-packing ($2\sqrt{6}/3$). The strain values ($\delta h=(3c/2a\sqrt{3})-1$) for the different films are summarized in Table 1. The weak values of the c/a ratio can be associated with strains which are essentially due to constrained one-dimensional shrinkage of the films normal to the substrate plane during the drying (removal of alcohol and water). Note also that the volume of the 3D-hexagonal unit cell continuously decreases by increasing the aging time of the silica sol. Finally, the evolution of the q_z coordinate appears as clearly equivalent to the $d_{(002)}$ spacing variations observed on the $\theta-2\theta$ diffraction patterns as a function of the condensation time. This is obviously related to the Bragg–Brentano geometry which allows one to explore the reciprocal space only along the z direction.

Furthermore, we studied films produced from diluted CTAB/sol in order to decrease their thickness (Table 2). Dilution was made just before deposition, and the aging time of the starting silica sol was 1 hour at 60 °C. This should lead to an emphasis of the domains located near the surface and consequently to an increase in the proportion of ordered regions with good texturing. The film thickness continuously decreases from 1300 to 40 nm when the dilution increases from 1 : 1 to 1 : 27. Fig. 4 shows the evolution of the 002 peak as a function of the dilution ratio for uncalcined films. We note a decrease in the $d_{(002)}$ spacing when the dilution increases (from 1 : 1 to 1 : 27). GISAXS patterns ($\alpha=\alpha_c+0.1°$, $z_o=400$ nm for a wavelength of 0.177 nm) show that this evolution comes from a reduction of the c/a ratio (up to 20%) which is mainly due to a contraction along the z direction (the c-hexagonal parameter varies from 8.0 to 6.2 nm). This suggests that the dilution and

Table 1 Uncalcined films prepared from silica sols with different aging times: structural parameters deduced from GISAXS patterns (q_y and q_z coordinates for the 011 and $0\bar{1}1$ peaks, δh strain value, c/a ratio and 3D-hexagonal unit cell volume) and from X-ray diffraction patterns performed in the Bragg–Brentano geometry (q_z coordinate is equal to $\pi/d_{(002)}$ for the 002 peak)

Aging time/h	q_y (GISAXS)/nm^{-1}	q_z (GISAXS)/nm^{-1}	q_z (XRD)/nm^{-1}	c/a	$\lvert\delta h\rvert$	Unit cell volume/nm^3
1	1.17	0.78	0.77	1.29	0.21	266
1.5	1.21	0.78	0.80	1.33	0.18	249
4.5	1.25	0.82	0.84	1.31	0.20	221
23		0.84	0.84			

Table 2 Uncalcined films prepared with diluted CTAB/sol mixtures: structural parameters deduced from GISAXS patterns (q_y and q_z coordinates for the 011 and $0\bar{1}1$ peaks, δh strain value, c/a ratio and 3D-hexagonal unit cell volume) and from X-ray diffraction patterns performed in the Bragg–Brentano geometry (q_z coordinate is equal to $\pi/d_{(002)}$ for the 002 peak)

Dilution	Thickness/nm	q_y (GISAXS)/nm^{-1}	q_z (GISAXS)/nm^{-1}	q_z (XRD)/nm^{-1}	c/a	$\lvert\delta h\rvert$	Unit cell volume/nm^3
1/1	1310	1.25	0.78	0.82	1.38	0.15	233
1/3	290	1.29	0.85	0.85	1.32	0.19	201
1/9	100	1.32	0.94	0.94	1.20	0.26	173
1/27	40	1.31	1.01	0.96	1.13	0.31	162

consequently the decrease of the film thickness is associated with the increase of the anisotropic strain effects during the drying.

GISAXS patterns (Fig. 5), at least for the three first dilutions (1 : 1, 1 : 3 and 1 : 9), exhibit Bragg spots showing that the silica sol belongs to the optimum condensation range. Besides Bragg spots corresponding to the [$2\bar{1}0$] zone axis orientation for the 3D hexagonal structure, the presence of high order diffraction spots related to the [010] zone axis orientation, such as $2\bar{1}2$, $\bar{2}12$, $2\bar{1}0$ and $\bar{2}10$, suggests a high degree of ordering for the spheres. This seems to be optimized in films of 300 nm thickness (dilution 1 : 3) for which both the intensity of the sharp 002 peak is the highest on the XRD pattern and the diffuse scattering intensity is the lowest on the GISAXS pattern. In the last diagram, there is no diffuse ring and only some weakly diffuse lines reflecting some disordered regions with an hexagonal local order. Finally, HRTEM observations (Fig. 6b) clearly show that the optimal dilution leads to well textured mesoporous films which exhibit an extended 3D-hexagonal order ranging over all the film thickness.

4 Discussion

All these results can be explained from a very simple model that allows interpretation of our experimental data using the competition between structuration and gelation of the film. Concerning the structuration, we have observed, as Ogawa and Kikuchi,[18] the necessity of fast alcohol removal. First, spin-coating in air is required, instead of a confined alcohol atmosphere, to obtain mesostructured films. Second, in our case, there is a clear correlation between the structuration and the ethanol concentration gradient during the drying, with a growth of ordered domains from the air–sol interface towards the interior of the film. The mechanism of formation of the 3D-hexagonal mesophase during the drying of the films is probably similar to the one previously proposed by Lu *e't al.*:[10] the removal of ethanol, preferentially at the air–sol interface, allows one to increase the concentration of CTAB and to exceed the critical micelle concentration. This leads to the successive formation of spherical micelles and their organization in a 3D-hexagonal mesophase by assembling silica–surfactant micellar species with the preorganized air–sol interfacial region.

The second important parameter is the solidification at the drying stage which stabilizes a certain degree of order in the mesostructured film. The chemical conditions were chosen in such a way that complete hydrolysis of TEOS occurs in a few minutes in the sol. The condensation is then realized separately from the hydrolysis with the formation of siloxane bridges [≡Si–O–Si≡] between the hydrolyzed species [≡Si–OH]. For the usual sol–gel transition at low pH, it is well known that the condensation can be split into different parts:[19,20] the first steps consist of a progressive assembling of small organized units (such as cyclic tetramers and polyhedral octamers). This is followed by a cluster aggregation phase which gives rise to fractal lacunar aggregates whose percolation leads to the gelation. Finally, drying by evaporation gives rise to capillary pressure that causes shrinkage of the gel network.

In our experiments of spin coating deposition, the formation of mesostructured films requires micellar organization and stabilization by gelation of a percolative silica network to constitute the wall structure. Due to the rapid removal of alcohol, the gelation results from percolation of lacunar fractal particles whose size is determined by the aging time of the acidic silica sol. The silica network then stabilizes the micellar organization existing in the sol at the moment of the percolation. A clear indication of the lacunar wall structure at the gelation is given by the reduction of the c/a ratio of the hexagonal lattice spacing after drying, which is deduced from GISAXS data. As expected, the shrinkage of the silica network is more marked when the aging time of the silica sol increases, *i.e.* when the size of the lacunar aggregates and consequently their porosity increase at the gelation. Obviously, the extension of the 3D-hexagonal order after drying significantly decreases when the formation of the wall structure is prevented. This is observed either for small fractal unit silica aggregates which are unable to form a percolative network, or for large units which

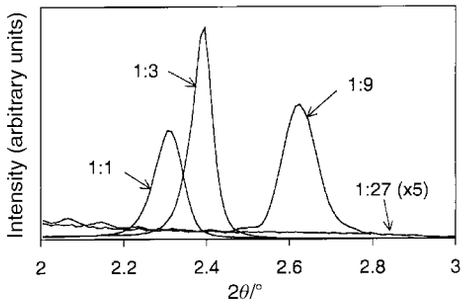

Fig. 4 X-Ray diffraction patterns recorded for films prepared with diluted CTAB/sol mixtures (ethanolic dilution from 1 : 1 to 1 : 27; aging time: 1 h at 60 °C).

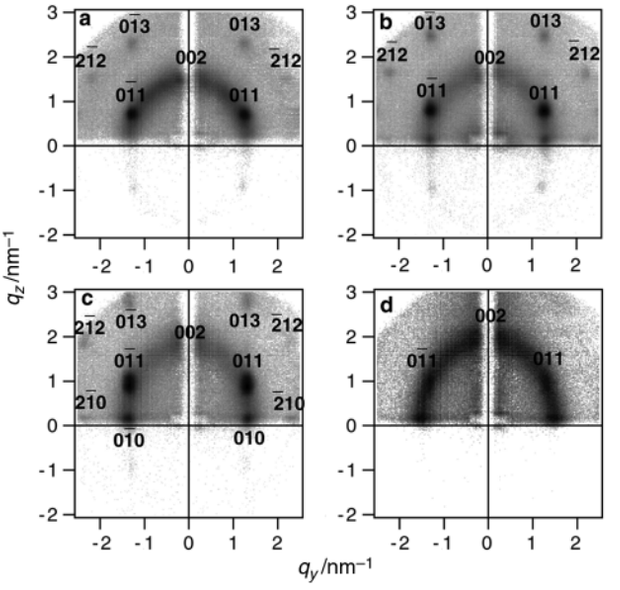

Fig. 5 GISAXS patterns recorded at $\alpha = \alpha_c + 0.1°$ for uncalcined mesostructured films prepared with diluted CTAB/sol mixtures. The ethanolic dilutions are 1 : 1 (a), 1 : 3 (b), 1 : 9 (c) and 1 : 27 (d). The aging time is 1 h at 60 °C.

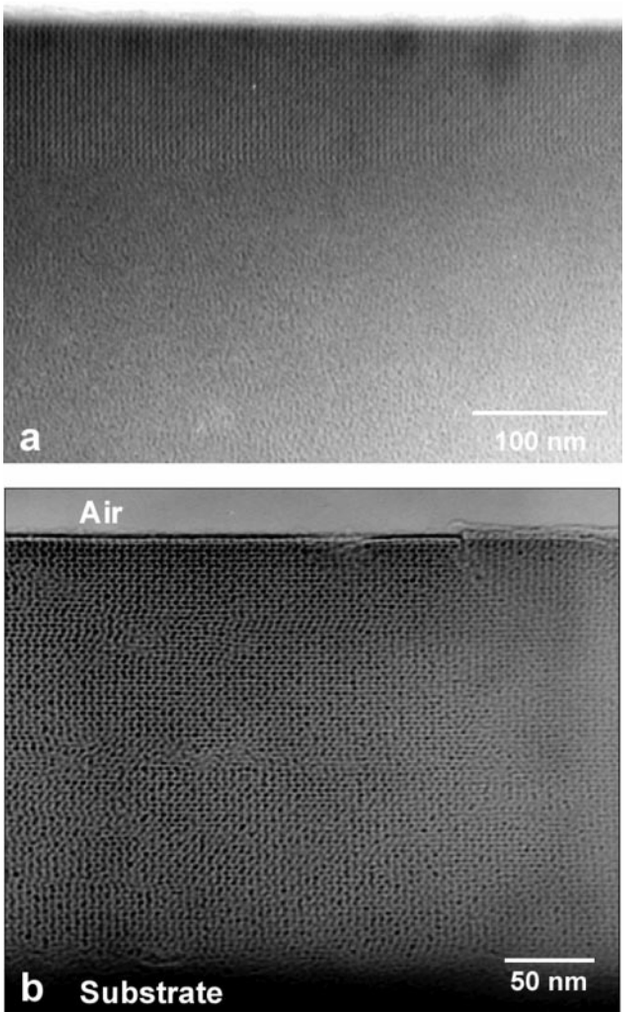

Fig. 6 HRTEM images of calcined mesoporous films prepared with different diluted CTAB/sol mixtures. (a) 650 nm film thickness (only the air–film interface is shown), (b) 250 nm film thickness. In (b), the (001) lattice fringes of the hexagonal structure described in ref. 12 are clearly visible within the whole film. In all cases, these fringes are parallel to the interface between the glass substrate and the porous silica film which indicates a strong texture of the film. This effect was also observed in plane view samples where all the domains are disoriented one from the others but have the [001] common direction.[12] By careful calibrations of the electron microscope magnification, the lattice parameter of this structure along the *c* axis was measured. It is equal to 3.1 nm which corresponds to the *c*/2 periodicity of the hexagonal structure. This value is in full agreement with the θ–2θ X-ray diffraction data.

are unable to occupy the space between spherical micelles without a large distortion of the hexagonal structure. This explains the optimum of condensation observed in our first series of experiments.

In the second series, we have demonstrated another way to extend the hexagonal order by diluting the CTAB/silica mixture. This decreases the film thickness and extends the well-textured region over all the sample. However, this also increases the anisotropy with a reduction of the *c*/*a* hexagonal ratio due to a contraction of the silica network mainly along the *z* direction as shown in GISAXS experiments. In fact, the observed optimum of dilution for the order extension simply corresponds to a critical value of the film thickness. Below about 300 nm, the extent of the hexagonal order is reduced both by the high distortion of the hexagonal structure (low value of the *c*/*a* ratio) and by the limited dimension along the *z* direction. Besides, the increase of the shrinkage and its anisotropy observed for the low thickness films could be understood in terms of anisotropic mechanical properties of the

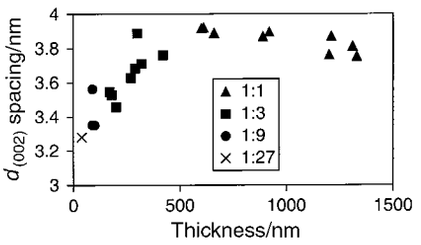

Fig. 7 $d_{(002)}$ spacing *versus* thickness for different films prepared by varying the dilution of the CTAB/sol mixture (from 1 : 1 to 1 : 27) or the angular velocity range of the spinner (from 1000 to 5000 rpm for the 1 : 1 and the 1 : 3 mixtures).

3D-hexagonal mesophase. For low thickness films (100–300 nm), the long range hexagonal order probably allows a cooperative contraction of the structure during the drying, which is enhanced along the *z* direction, *i.e.* perpendicular to the hexagonal basal plane. In contrast, for the high thickness films (1 μm), the disordered regions formed from domains with different orientations could prevent this cooperative shrinkage, reducing the contraction and its anisotropy in small ordered regions. A third series of experiments shows that the contraction along the *z* direction increases when the thickness of the film is also decreased by changing the coating speed (Fig. 7). This confirms that, in our diluting experiments, the observed behavior is only due to the film thickness, and not to other consequences of the concentration change. Note also the presence of a plateau for the μm-thick films which confirms the buffer action of disordered regions for the contraction in ordered 3D-hexagonal regions.

5 Conclusion

In summary, mesostructured films deposited on glass substrates by spin coating generally present a gradient of ordering, with a 3D-hexagonal mesophase near the surface and a disordered micellar structure at the interior. Two parameters are shown to critically determine the overall quality of the films. The first is the size of the silica units in the starting sol, which allows the formation of a percolative silica network constituting the wall structure in the mesophase. The second is the film thickness which emphasizes the well-textured region near the surface and limits the distortion of the hexagonal structure at the drying. Finally, the optimization of these two parameters, *via* the adjustment of the deposited solution, allows one to extend the 3D-hexagonal ordering and the texturing over all the film thickness.

Acknowledgements

Appreciation is expressed to the LURE for the use of its experimental facilities and to O. Lyon and A. Naudon for their invaluable collaboration during GISAXS measurements. The LURE is the Laboratoire pour l'Utilisation du Rayonnement Electromagnétique, 91405 Orsay (France).

References

1 J. S. Beck, J. C. Vartuli, W. J. Roth, M. E. Leonowicz, C. T. Kresge, K. D. Schmitt, C. T.-W. Chu, K. H. Olson, E. Sheppard, S. B. McCullen, J. B. Higgins and J. L. Schlenk, *J. Am. Chem. Soc.*, 1992, **114**, 10834.
2 J. S. Beck and J. C. Vartuli, *Curr. Opin. Solid State Mater. Sci.*, 1996, **1**, 76.
3 Q. Huo, D. I. Margolese and G. D. Stucky, *Chem. Mater.*, 1996, **8**, 1147.
4 N. K. Raman, M. T. Anderson and C. J. Brinker, *Chem. Mater.*, 1996, **8**, 1682.
5 D. Zhao, J. Feng, Q. Huo, N. Melosh, G. H. Fredrickson, B. F. Chmelka and G. D. Stucky, *Science*, 1998, **279**, 548.

6 H. Yang, N. Coombs, I. Sokolov and G. Ozin, *Nature*, 1996, **381**, 589.
7 I. A. Aksay, M. Trau, S. Manne, I. Honma, N. Yao, L. Zhou, P. Fenter, P. M. Eisenberg and S. M. Gruner, *Science*, 1996, **273**, 892.
8 M. Ogawa, *J. Am. Chem. Soc.*, 1994, **116**, 7941.
9 M. Ogawa, *Chem. Commun.*, 1996, 1149.
10 Y. Lu, R. Gangull, C. A. Drewlen, M. T. Anderson, C. J. Brinker, W. Gong, Y. Guo, H. Soyez, B. Dunn, M. H. Huang and J. I. Zink, *Nature*, 1997, **389**, 364.
11 D. Zhao, P. Yang, N. Melosh, J. Feng, B. F. Bradley, F. Chmelka and G. D. Stucky, *Adv. Mater.*, 1998, **10**, 1380.
12 S. Besson, C. Ricolleau, T. Gacoin, C. Jacquiod, J. P. Boilot, *J. Phys. Chem. B*, submitted.
13 A. Naudon and D. Babonneau, *Z. Mettallkd.*, 1997, **88**, 596.
14 S. A. Holt, G. J. Foran and J. W. White, *Langmuir*, 1999, **15**, 2540.
15 R. Ryoo, J. M. Kim, C. H. Ko and C. H. Shin, *J. Phys. Chem.*, 1996, **100**, 17718.
16 R. Ryoo, C. H. Ko, S. J. Cho and J. M. Kim, *J. Phys. Chem. B*, 1997, **101**, 10610.
17 R. Ryoo, J. M. Kim, S. J. Cho and C. H. Ko, *Microporous Mesoporous Mater.*, 1998, **21**, 235.
18 M. Ogawa and T. Kikuchi, *Adv. Mater.*, 1998, **10**, 1077.
19 C. J. Brinker and G. W. Scherer, in *Sol–Gel Science*, Academic Press, San Diego, 1990.
20 F. Devreux, J.-P. Boilot, F. Chaput and A. Lecomte, *Phys. Rev. A*, 1990, **41**, 6901.